ISSN 2079-1704. Хімія, фізика та технологія поверхні. 2025. Т. 16. № 1. С. 3-17

PACS: 31.15.A-; 31.15.bu; 31.15.E-; 31.70.Dk; 36.40.-c doi: 10.15407/hftp16.01.003

V.M. Gun'ko

MODELING OF BINARY NANOOXIDES WITH SOLID SOLUTIONS AND MIXED PHASES

Chuiko Institute of Surface Chemistry of National Academy of Sciences of Ukraine
17 General Naumov Str., Kyiv, 03164, Ukraine, E–mail: vlad_gunko@ukr.net

The electronic structure of individual metal (Ti, Al) or metalloid (Si) oxides as well as complex (binary, ternary, etc.) oxides is of importance from a practical point of view. In various applications of these materials as catalysts, sorbents, carriers, fillers, etc., the bandgap, polarizability, conductivity, and dielectric characteristics play a crucial role in the application efficiency. Therefore, accurate determination of these characteristics is strongly required. Sometimes theoretical determination of the characteristics is simpler, especially for large series of complex materials with varied compositions, by using quantum chemical methods (i.e., computations without synthesis) than experimental ones (synthesis and measurements). Upon computations with quantum chemical methods, selection of a method adequate to a task is important to obtain more accurate information. Therefore, in this study, two semiempirical methods (PM7 and DFTB+ used in semiempirical packages (MOPAC, DFTB+) and implemented in the most known packages such as Gaussian, GAMESS, AMS, etc.) have been used in parallel to DFT (mainly ωB97X–D/cc–pVDZ) to compute various clusters (22, 35, 88, 94, and 111 units) with silica, alumina, titania, titania/silica, and alumina/silica. The computations show that the bandgap value (E_g) of titania is mostly accurately computed with DFTB+ using cluster and periodic boundary conditions approaches. However, for other systems, the DFTB+ E_g values are typically underestimated. The PM7 and DFT bandgap values are more appropriate with the use of the potential approach V^{-1} (computation of the virtual levels of the systems with removed one electron) giving E_{g1}. Detailed analysis of the integral density of electron states and density of atomic charges summarized by atom types reveals several reasons of nonmonotonic changes in the E_g values vs. composition of binary oxides. As a whole, the PM7 and DFT methods give correct tendencies in the changes in the E_g and E_{g1} values vs. binary oxide compositions, but the E_g values are typically overestimated in contrast to underestimated values by DFTB+. Water adsorbed in a low amount on oxide clusters provides a significant stabilization of a surface since the Gibbs free surface energy strongly decreases especially for titania-containing systems. This explains more effective adsorption of water from air onto nonporous binary oxides or titania in comparison to silica.

Keywords*: binary nanooxides, solid solution, mixed phases, electronic structure, DFT method, semiempirical quantum chemical methods*

INTRODUCTION

The characteristics of complex oxides, *e.g.*, titania/silica (TS) and alumina/silica (AS), depend not only on the content of each phase but also on a distribution type of each oxide in the complex systems [1–7]. There are several possible distributions: (i) solid solution of a guest phase (minor) in a host one with remained lattice features of the latter; (ii) mixed pure phases with weak or tight contacts between them in aggregate particles; (iii) combination of the first and second distribution types in complex particles; (iv) core–shell particles with the cores and shells composed of different oxides; and (v) a blend of independent particles, *e.g.*, mechanically treated blend of individual oxides. The binary oxide systems could be simultaneously synthesized, prepared with two individual oxides, or deposited one oxide on particles of another one. These preparation methods strongly affect the characteristics and properties of the final materials [1–8]. The phase distribution type in complex oxides affects the nature of active surface sites including acidic (Brønsted acid sites) and basic hydroxyls, Lewis acid (incomplete O–coordinated metal ions) and basic (surface O) sites, electron band structure, *etc*. All these aspects are of importance on practical applications of the oxide materials [1–8].

There are many various well-known quantum chemical (QC) methods such as *ab initio*, density functional theory (DFT) [9–16], and effective semiempirical approaches such as PM7, PM6 [17], DFTB+ [18], *etc*. The latter are used not only in MOPAC [17] (http://openmopac.net/) and DFTB+ [18] (https://dftbplus.org/index.html) packages but also in well-known QC program

suits: Gaussian [19] (https://gaussian.com/gaussian16/), GAMESS [20] (https://www.msg.chem.iastate.edu/gamess/), AMS [21] (http://www.scm.com) and others (see https://en.wikipedia.org/wiki/List_of_quantum_chemistry_and_solid-state_physics_software). As a whole, the QC methods are the effective tools to analyze many important characteristics of various materials including mentioned oxides using cluster and periodic boundary conditions (PBC) approaches [9–16]. Note that the PM7 and DFTB+ methods are characterized by very different parametrization methodology, since in PM7, each atom is parametrized *per se*, but in DFTB+, each pair of atoms is parametrized. This difference (as a reason of selection and comparison of these methods) could affect the calculation errors. As a whole, for each characteristic of each system, a more appropriate method could be found. For example, to estimate the bandgap between the valence (VB) and conduction (CB) bands, the PBC could be more appropriate than the cluster approach, since there is a dependence of the VB and CB structure and width (*e.g.*, band broadening for larger clusters or particles due to the Pauli exclusion principle for electrons) on the cluster sizes. For some local characteristics related to, *e.g.*, active surface sites, the cluster (especially with DFT and appropriate basis sets) approaches could be more appropriate than PBC one due to some features of the latter (*e.g.*, a cell should be strongly expanded to reduce site-site interactions and the PBC could be used only in two directions). It should be noted that semiempirical methods (*e.g.*, PM6, PM7, DFTB+, *etc*.) could be more appropriate than DFT or *ab initio* ones to study large systems with several thousands of atoms due to much smaller required computational resources for the former [6–16].

According to experimental data [22–32], the bandgap between VB and CB changes for individual oxides studied here from E_g = 9.0±0.2 eV (amorphous silica) and 6.7±0.2 eV (γ–Al_2O_3) as dielectrics and 3.2 eV for anatase as a semiconductor that also depends on the particulate morphology. The bandgap of binary oxides depends also on additional factors including phase contents and distributions, particle shape and sizes, coherent scattering region sizes, *etc*. There is a tendency of changes in E_g closer to that of an individual material with smaller one. For example, for TS, it is between 3.5 and 4 eV [23–38] that is much closer to the E_g value of titania than silica. This is due to a relatively low concentration threshold for electron percolation in binary nanostructured systems that could be about 10 % for titania with random phase distribution in TS [6–8]. However, for core-shell particles, the E_g value should correspond to that of the shell.

As a whole, the electronic structure changes influence the application efficiency of the materials [39–46]. Therefore, in this study, various solid solutions and tightly contacted phases were modeled for binary oxides (TS and AS) to analyze the effects on the bandgap, integral density of electron states, and charge distribution functions compared to that of individual oxides. Note that for initial structures, individual silica was modeled as amorphous one, alumina represented γ–Al_2O_3, and titania was anatase. Thus, the aim of this study was to compare the characteristics of individual silica, alumina (γ–Al_2O_3), and titania (anatase) and related binary oxides TS and AS (random distributions of a guest phase (minor) with isomorphic substitution of metal atoms in a host phase (with remained lattice features) by metal atoms of the guest phase) with solid solutions of silica in titania (anatase), titania in silica (amorphous), and alumina in silica (amorphous) computed using different methods such as DFT [13–16], DFTB+ [18], and PM7 [17] using different QC program suits (all are the latest Linux versions) to show some their advances and limitations. Additionally, a model of AS particle includes two attached fragments of silica (amorphous) and γ–Al_2O_3.

COMPUTATION METHODS

Several types of silica, titania, alumina, TS, and AS clusters (with random distributions of a guest phase) with 22, 35, 88, 94, and 111 units (with surface hydroxyls to provide zero formal charge) were used in QC computations. QC calculations of the clusters using the DFT method were carried out using a hybrid functional ωB97X–D with the cc–pVDZ basis set with the Gaussian 16 C.02 [19], GAMESS 2023 R2 and 2024 R2 patch 1 [20], and AMS 2023.1 and 2024.1 [21] program suits. For a silica cluster (35 units), B3LYP/cc–pVDZ and B3LYP/6-31G(d,p) were also used to compare with

ωB97X–D/cc–pVDZ (note that these basis sets are similar, *e.g.*, for this silica cluster, a number of basis functions/primitive gaussians is 2140/4494 (6–31G(d,p)) and 2018/5594 (cc–pVDZ)). The solvation effects were analyzed using the SMD method [47]. To compute the Gibbs free energy of solvation $\Delta G_s = G_l - G_g$, where G_l and G_g are the Gibbs free energies of a molecule free or bound to silica cluster in the liquid and gaseous media, respectively. The calculations were performed taking into account zero–point and thermal corrections to the Gibbs free energy in the gas phase and for solved molecules and clusters with the geometry optimized using ωB97X–D/cc–pVDZ. The cluster models or the systems with periodic boundary conditions (PBC) were also calculated using the DFTB+ (ver. 24.1) [18] (with some additional parameters [48]) and PM7 (MOPAC, ver. 22.1.1) [17] methods. All DFT and semiempirical computations were carried out using the latest Linux versions of the programs [17–21]. Preparation of initial cluster structures and visualization of the calculation results were carried out using several programs [49–52]. The system geometry was optimized in all the cases.

Note that according to previous investigations [53–58], for relatively correct calculations of the electronic structure of the oxide systems, a minimal size of oxide clusters should correspond to at least 20 units. Therefore, the minimal clusters used here include 22 units. However, in the case of PBC calculations, an expanded cell of anatase includes 16 units.

The distribution functions of some parameters have been calculated with a simple equation [56–58]

$$f_n(X) = (2\pi\sigma_n^2)^{-0.5} \sum_j \frac{\exp[-(X_{n,j} - X)^2]}{2\sigma_n^2}, \quad (1)$$

where j is the number of a certain type (n) of atoms, σ^2 is the distribution dispersion, and X_j is the value of atomic charge (CDF) or electron energy of molecular orbitals, MO (integral density of electron states, IDES), and X is the current value.

Upon computing the MO levels in the conduction band (virtual levels), there is a systematic error in the MO energies due to completely filled electronic shells related to VB, *i.e.*, the absence of the effect of electron transfer from the valence band to CB on the potential field (*i.e.*, VB is completely infilled, but CB is completely empty). This results in too large E_g values due to overestimated energy of CB bottom. To correct this error, the CB could be computed for the charged system (q = +1 a.u.) with one removed electron (potential approach V^{-1} for CB). This correction could be used for the lowest virtual MO (LUMO1, Tables 1–3) to estimate the bandgap (E_{g1}) as the gap between the highest occupied MO, HOMO for uncharged system and lowest unoccupied MO, LUMO1 for charged system, as well as corrected IDES (IDES1) as a sum of two parts related to VB (IDES for occupied levels) and CB (IDES for corrected virtual levels with the approach V^{-1} for CB).

RESULTS AND DISCUSSION

The bandgap is an important characteristic for catalysts (*e.g.*, redox reactions are stimulated by electron transfer from a photocatalyst to reaction species that is more effective if the bandgap is narrower and the reactions could be occurred under not only ultraviolet but also visible light) and adsorbents (due to enhanced polarization effects for materials with smaller E_g values, *e.g.*, titania or titania/silica in comparison to silica [6, 59] compared upon interaction with water, *vide infra*). Therefore, the theoretical modeling of the electron band structures, especially upper valence (top, Fermi level), conduction (bottom), and forbidden (width) ones, should be accurate to predict important characteristics of complex materials. Here, the important boundary electron level energies (Tables 1–3), IDES (Figs. 1, 2, 6 *a*), and CDF (Figs. 3–6) are compared for titania, silica, alumina, titania/silica, and alumina/silica models computed using semiempirical PM7 and DFTB+ or density functional theory methods.

For anatase, the best results (with respect to the experimental data) for E_g are obtained with DFTB+ (both PBC and cluster models with the errors ΔE_g = 0.2 eV and 0.3 eV, respectively) (Table 2). The E_{g1} vales for anatase computed using the cluster approach with PM7 (Table 1) and DFT (Table 3) methods are worse (overestimated at ΔE_{g1} = 1.1 eV and 1.8 eV, respectively) than that of E_g by DFTB+ (Table 2) in comparison to the experimental E_g value of 3.2 eV. The PBC calculation of anatase with PM7 does not give a better E_g value than that in the cluster approach (Table 1).

Table 1. Energies of HOMO and LUMO and bandgap values (PM7)

Cluster	E_{HOMO} (eV)	E_{LUMO} (eV)	E_{LUMO1} (eV)	E_g (eV)	E_{g1} (eV)
$Ti_{16}O_{32}$(PBC)	–6.989	0.010		6.999	
$Ti_{22}O_{49}H_{10}$	–9.089	–2.215	–4.792	6.874	4.297
$Ti_{21}SiO_{49}H_{10}$	–9.209	–2.222	–4.240	6.987	4.969
$Ti_{20}Si_2O_{49}H_{10}$	–9.147	–2.279	–4.413	6.868	**4.734**
$Ti_{18}Si_4O_{49}H_{10}$	–9.523	–1.975	–4.219	7.548	5.304
$Ti_{16}Si_6O_{49}H_{10}$	–9.501	–1.890	–4.050	7.611	5.451
$Ti_{15}Si_7O_{49}H_{10}$	–9.862	–2.181	–4.868	7.681	4.994
$Ti_{11}Si_{11}O_{49}H_{10}$	–9.533	–1.761	–4.041	7.772	5.492
$Ti_8Si_{14}O_{49}H_{10}$	–9.795	–1.815	–4.546	7.980	5.249
$Si_{35}O_{87}H_{34}$	–11.013	0.060	–4.048	11.073	6.965
$Si_{88}O_{196}H_{40}$	–10.636	–1.403	–4.440	**9.233**	6.196
$Si_{88}O_{196}H_{40}@7H_2O$	–10.609	–1.312	–4.084	**9.297**	6.525
$Si_{82}Ti_6O_{196}H_{40}@7H_2O$	–9.493	–1.429	–2.873	8.064	6.620
$Si_{82}Al_6O_{196}H_{46}@10H_2O$	–10.072	–1.570	–3.929	8.502	6.143
$Al_{111}O_{189}H_{45}$	–9.913	–0.562	–6.815	9.351	3.098
$Al_{111}O_{189}H_{45}@6H_2O$	–10.019	0.389	–1.354	10.408	8.665

Note. $E_g = E_{LUMO} - E_{HOMO}$. E_{LUMO1} was calculated using the V^{-1} approach and $E_{g1} = E_{LUMO1} - E_{HOMO}$ (bold and underlined values are best ones close to experimental data)

Table 2. Energies of HOMO and LUMO and bandgap values (DFTB+)

Cluster	E_{HOMO} (eV)	E_{LUMO} (eV)	E_g (eV)
$Ti_{16}O_{32}$(PBC)	–2.559	0.874	**3.433**
$Ti_{22}O_{49}H_{10}$	–5.942	–2.447	**3.495**
$Ti_{21}SiO_{49}H_{10}$	–6.021	–3.419	2.602
$Ti_{20}Si_2O_{49}H_{10}$	–6.257	–3.246	3.011
$Ti_{18}Si_4O_{49}H_{10}$	–6.354	–5.217	1.137
$Ti_{16}Si_6O_{49}H_{10}$	–6.526	–5.085	1.441
$Ti_{15}Si_7O_{49}H_{10}$	–6.511	–5.128	1.383
$Ti_{11}Si_{11}O_{49}H_{10}$	–6.473	–5.243	1.230
$Ti_8Si_{14}O_{49}H_{10}$	–7.388	–5.746	1.642
$Si_{35}O_{87}H_{34}$	–8.170	–3.122	5.048
$Si_{88}O_{196}H_{40}$	–8.183	–4.153	4.030
$Si_{88}O_{196}H_{40}@7H_2O$	–7.894	–4.071	3.823
$Si_{82}Ti_6O_{196}H_{40}@14H_2O$	–5.780	–5.155	0.625
$Si_{82}Ti_6O_{196}H_{40}@14H_2O$*	–4.258	–3.804	0.454
$Si_{76}Ti_{12}O_{196}H_{40}@14H_2O$	–6.683	–5.114	1.569
$Si_{74}Ti_{14}O_{196}H_{40}@15H_2O$	–6.959	–5.200	1.759
$Si_{82}Al_6O_{196}H_{46}@10H_2O$	–6.902	–4.239	2.663
$Si_{76}Al_{12}O_{196}H_{52}@10H_2O$	–6.928	–4.812	2.116
$Si_{74}Al_{14}O_{196}H_{54}@10H_2O$	–7.135	–4.268	2.867
$Si_{72}Al_{16}O_{196}H_{56}@10H_2O$	–6.864	–3.983	2.881
$Al_{49}Si_{45}O_{198}H_{69}$	–6.323	–4.180	2.143
$Al_{111}O_{189}H_{45}$	–5.170	–4.002	1.168
$Al_{111}O_{189}H_{45}$*	–4.852	–2.523	2.329
$Al_{111}O_{189}H_{45}@6H_2O$	–6.180	–2.224	3.956

Note. *DFT geometry

For amorphous silica (modeled by a cluster with 88 units), the best result is obtained with PM7 (Table 1, E_g at $\Delta E_g = 0.1$ eV). For DFT, the V^{-1} approach could improve the bandgap value (Table 3, E_{g1} at $\Delta E_{g1} = 1$ eV and E_g at $\Delta E_g \approx 1.5$ eV) in contrast to that of PM7 (Table 1, E_{g1} at $\Delta E_{g1} \approx -3$ eV). An increase in silica cluster from 35 to 88 units results in a decrease (by *ca*.

1 eV) in the E_g value calculated by all methods (Tables 1–3) that is due to the Pauli exclusion principle for electrons. For a dry γ–Al_2O_3 cluster with 111 units, DFT gives a better result (Table 3, E_g at $\Delta E_g = -0.5$ eV) than PM7 (Table 1, overestimated E_g at $\Delta E_g = 2.6$ eV) or DFTB+ (Table 2, underestimated E_g at $\Delta E_g = -5.5$ eV). Hydration of both silica and alumina clusters results in certain broadening of the bandgap calculated by all methods. This could be considered as a result of surface relaxation with decreasing free surface energy (surface atoms are predominant for the clusters studied; therefore, their state can strongly affect all the characteristics of the systems).

Table 3. Energies of HOMO and LUMO and bandgap values (DFT with ωB97X–D/cc–pVDZ)

Cluster	E_{HOMO} (eV)	E_{LUMO} (eV)	E_{LUMO1} (eV)	E_g (eV)	E_{g1} (eV)
$Ti_{22}O_{49}H_{10}$	–10.729	–1.634	–5.638	9.095	5.091
$Ti_{21}SiO_{49}H_{10}$	–10.681	–1.761	–4.483	8.920	6.198
$Ti_{18}Si_4O_{49}H_{10}$	–10.835	–1.760	–4.357	9.075	6.478
$Ti_{16}Si_6O_{49}H_{10}$	–10.888	–1.730	–4.110	9.158	6.778
$Ti_{15}Si_7O_{49}H_{10}$	–10.683	–1.815	–4.498	8.868	6.185
$Ti_{11}Si_{11}O_{49}H_{10}$	–9.725	–1.712	–4.248	8.013	5.477
$Ti_8Si_{14}O_{49}H_{10}$	–9.735	–1.665	–4.181	8.070	5.554
$Si_{35}O_{87}H_{34}$	–10.721	1.100		11.821	
$Si_{35}O_{87}H_{34}$*	–8.353	–0.970		7.383	
$Si_{35}O_{87}H_{34}$**	–8.252	–0.651		7.601	
$Si_{88}O_{196}H_{40}$	–10.526	0.232	–2.612	10.758	7.914
$Si_{88}O_{196}H_{40}@7H_2O$	–10.530	0.336	–2.271	10.866	8.259
$Si_{82}Ti_6O_{196}H_{40}@7H_2O$	–9.194	–1.060	–2.199	8.134	6.995
$Si_{76}Ti_{12}O_{196}H_{40}@14H_2O$	–9.754	–1.076	–3.494	8.678	6.260
$Si_{82}Al_6O_{196}H_{46}@10H_2O$	–10.177	0.043	–2.358	10.220	7.819
$Si_{76}Al_{12}O_{196}H_{52}@10H_2O$	–10.086	–0.012	–3.494	10.074	**6.592**
$Si_{74}Al_{14}O_{196}H_{54}@10H_2O$	–10.149	0.074	–2.372	10.223	7.777
$Si_{72}Al_{16}O_{196}H_{56}@10H_2O$	–9.999	0.107	–1.939	10.106	8.060
$Al_{49}Si_{45}O_{198}H_{69}$	–9.441	–0.139	–1.882	9.302	**7.559**
$Al_{111}O_{189}H_{45}$	–7.104	–0.912	–4.200	**6.192**	2.904
$Al_{111}O_{189}H_{45}@6H_2O$	–8.689	–0.491	–1.824	8.198	**6.865**

Note. *B3LYP/cc–pVDZ. **B3LYP/6–31G(d,p). E_{LUMO1} was calculated using the V^{-1} approach and $E_{g1} = E_{LUMO1} - E_{HOMO}$, but $E_g = E_{LUMO} - E_{HOMO}$

As a whole, there are certain tendencies in the bandgap changes depending on the binary oxide compositions (Tables 1–3, Figs. 1 and 2). An increase in the silica (guest phase as a solid solution with random distributions) content in the anatase cluster with 22 units results in bandgap broadening by *ca*. 1 eV (PM7, Table 1). This is in agreement with experimental data [36–38]. The DFT calculations (Table 3) demonstrate rather opposite results for the E_g (decreasing in comparison to E_g for pure anatase cluster) and E_{g1} (increasing) values with nonmonotonic changes. For an AS cluster $Al_{49}Si_{45}O_{198}H_{69}$ with tight contact between two pure phases, the value of E_{g1} (DFT, Table 3) is between the experimental values for silica and alumina (average weighted values is 7.801). The appearance of titania in a silica cluster with 88 units (solid solution with random distributions) leads to the opposite results in comparison to that for silica in titania, *i.e.*, the value of E_g decreases with increasing titania content (Tables 1 and 3) that is in agreement with the experimental data [36–38]. However, these changes are rather nonmonotonic because there are several effects (sometimes opposite): (i) appearance of the guest atoms (Si in titania or Al and Ti in silica) and an increase in their content leads to enhanced stress of the lattice and changes in the lattice constants; (ii) changes in the electron density location (*e.g.*, $q_{Si} > q_{Al}$, Figs. 3–5) and an increase in the heterogeneity of the charge distributions (Figs. 3–5); (iii) appearance of the bridging hydroxyls in AS that are absent in silica; (iv) certain inconsistency in the characteristics (valence, size, charge) of the guest atoms to those of the host ones; and (v) enhanced changes in IDES (Figs. 1 and 2).

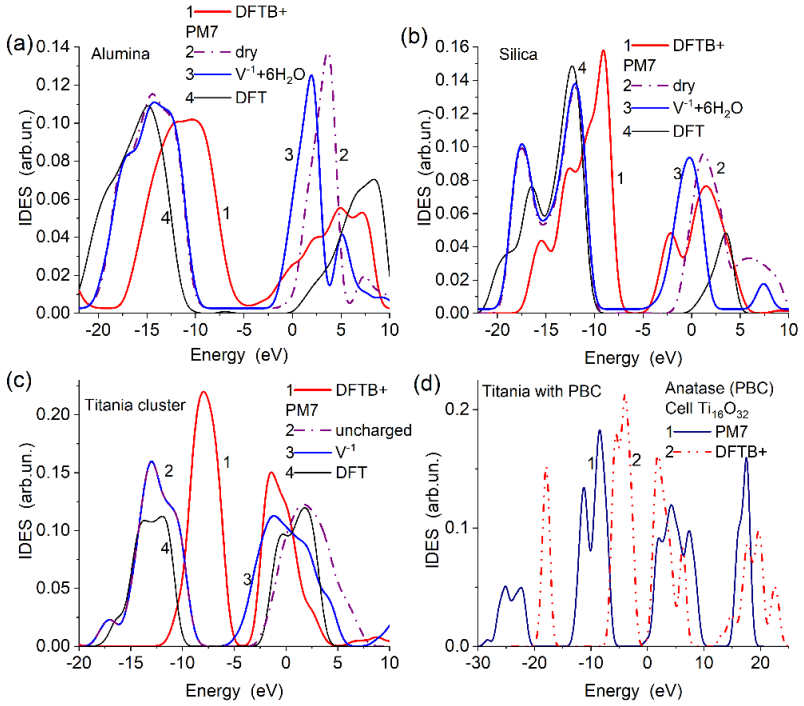

Fig. 1. IDES (in upper VB and lower CB) calculated with DFT, DFTB+, and PM7 methods for (*a*) alumina (dry $Al_{111}O_{189}H_{45}$ and wetted $Al_{111}O_{189}H_{45}$@$6H_2O$), (*b*) silica (dry $Si_{88}O_{196}H_{40}$ and wetted $Si_{88}O_{196}H_{40}$@$7H_2O$), (*c*, *d*) titania (*c*) $Ti_{22}O_{49}H_{10}$ and (*d*) $Ti_{16}O_{32}$ with PBC

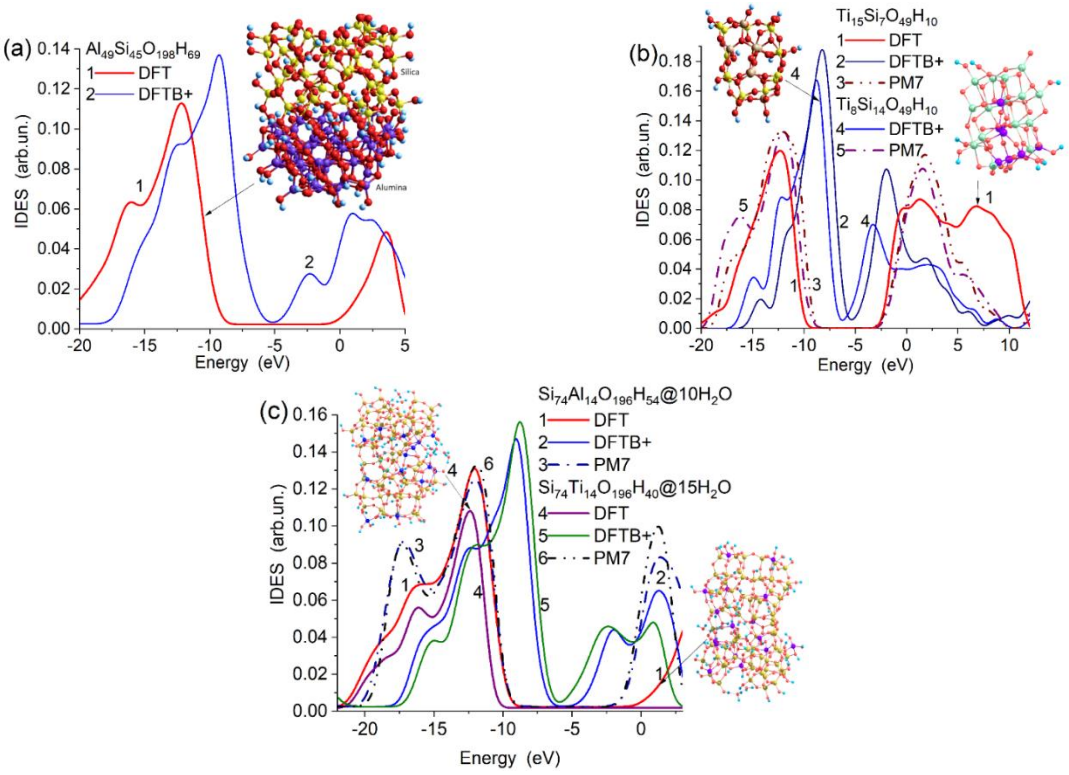

Fig. 2. IDES (in upper VB and lower CB) calculated with DFT, DFTB+, and PM7 methods for (*a*) alumina/silica with individual phases, (*b*) titania/silica with silica embedded into the anatase cell, (*c*) alumina/silica and titania silica with alumina and titania embedded into amorphous silica matrix

It should be noted that the DFTB+ method gives relatively poor (underestimated) results for E_g for all systems with exception of anatase (Table 2) due to too high Fermi levels and too low CB bottom levels (Table 2, Figs. 1 and 2). However, the DFTB+ method could give better results for the Fermi level (E_{HOMO}) *per se* than that for the CB bottom (E_{LUMO}) in contrast to the DFT method giving the opposite results with too deep Fermi levels. These results could be explained by non-optimal pair m_1–m_2 (m_x = Ti, Si, Al) parameters [48]. As a whole, the PM7 and DFT E_{g1} values better (mainly less overestimated) correspond to the experimental values than the PM7 and DFT E_g ones, which are more strongly overestimated (Tables 1 and 3) in comparison to the experimental data.

Typically, the DFTB+ IDES (Figs. 1 and 2) shift toward higher levels for VB and lower levels for CB than that of PM7 and DFT IDES. However, in the case of the V^{-1} approach (for the clusters) with PM7, the CB bottom is close to that of DFTB+ (Fig. 1), as well as in the case of PBC calculations of anatase (Fig. 1 *d*). The top of the upper VB is linked to the electrons located on the oxygen atoms (*i.e.*, Lewis base sites) due to the abundance of the electron density on the O atoms (Figs. 3 *b*, 4 *b*, and 5 *b*, *f*). The bottom of the CB is linked to metal atoms with maximum positive charges (*i.e.*, Lewis acid sites) (Figs. 3 *c*–*e*, 4 *c*, *d*, and 5 *c*, *d*, *g*, *h*). However, there is no simple correlation between the boundary IDES functions (Figs. 1 and 2) and Mulliken charge distributions on the O and metal atoms (Figs. 3–6) calculated using DFTB+ and PM7 or DFT methods.

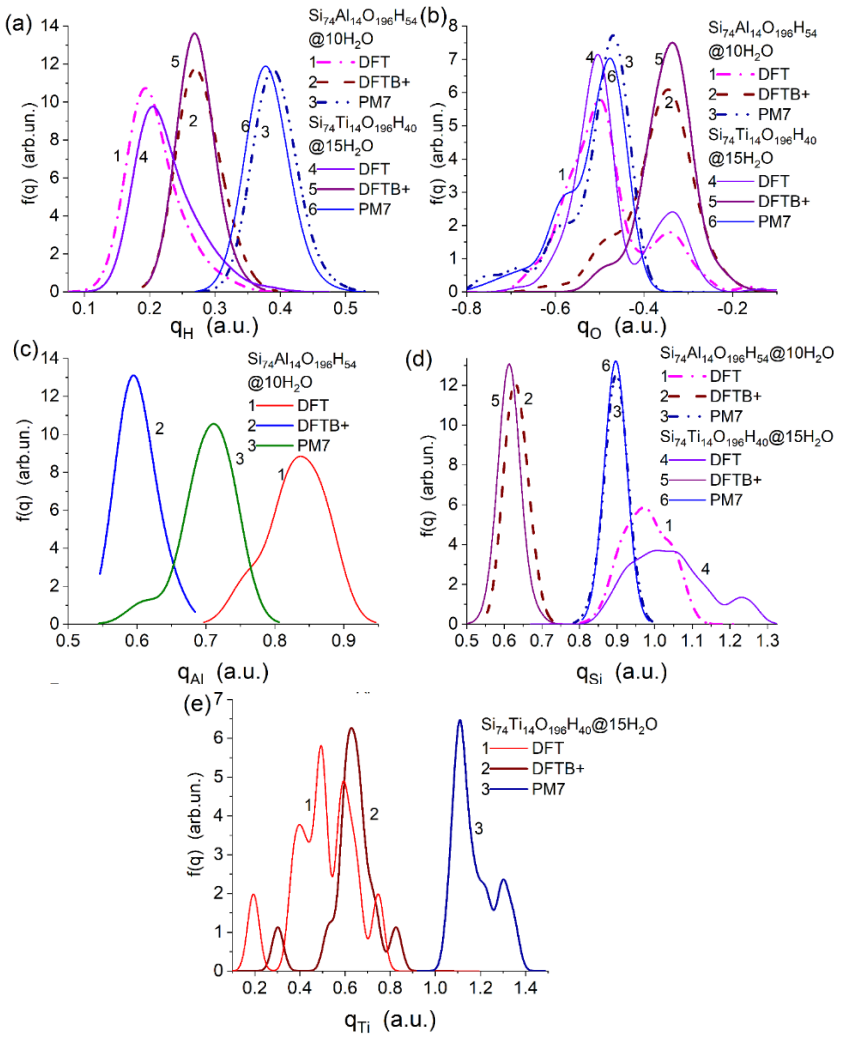

Fig. 3. Mulliken charge value distributions on (*a*) H, (*b*) O, (*c*) Al, (*d*) Si, and (*e*) Ti atoms in the clusters $Si_{74}Al_{14}O_{196}H_{54}$@$10H_2O$ and $Si_{74}Ti_{14}O_{196}H_{40}$@$15H_2O$ calculated using DFT, DFTB+, and PM7 methods

This could be explained by the method of the estimation of the Mulliken charges [9–14] for electron-donor (H, Al, Si, Ti) and electron-acceptor (O) atoms forming significantly polar bonds in metal (*e.g.*, Al and Ti) or metalloid (Si) oxides, as well as by changes in the lattice stress *vs.* composition of binary oxides leading to the appearance of the O, Al, Si, and Ti atoms with different charges (therefore, the CDF have complex shapes, Figs. 3–5). Note that the adsorbed water molecules more strongly affect (stabilize) the CB than VB (Fig. 1 *a*–*c*) since the CB bottom shifts by *ca*. 2 eV toward lower energies.

The maximum CDF location for certain atoms more strongly depends on the methods (and basis sets) type than on the cluster composition (Figs. 3–6). Therefore, selection of a method (and basis set) for calculations of the oxide cluster models could be more important than the sizes (upper the size threshold of 20 units) of the clusters. Additionally, appropriate selection of both methods (and basis sets) and models could allow one to obtain most corrected results. However, there are no universal rules to do that because of the existence of many-factor effects on the calculation results. Therefore, comparison of computation results to experimental data could be used as the main criterion for selection of methods (and basis set) and models.

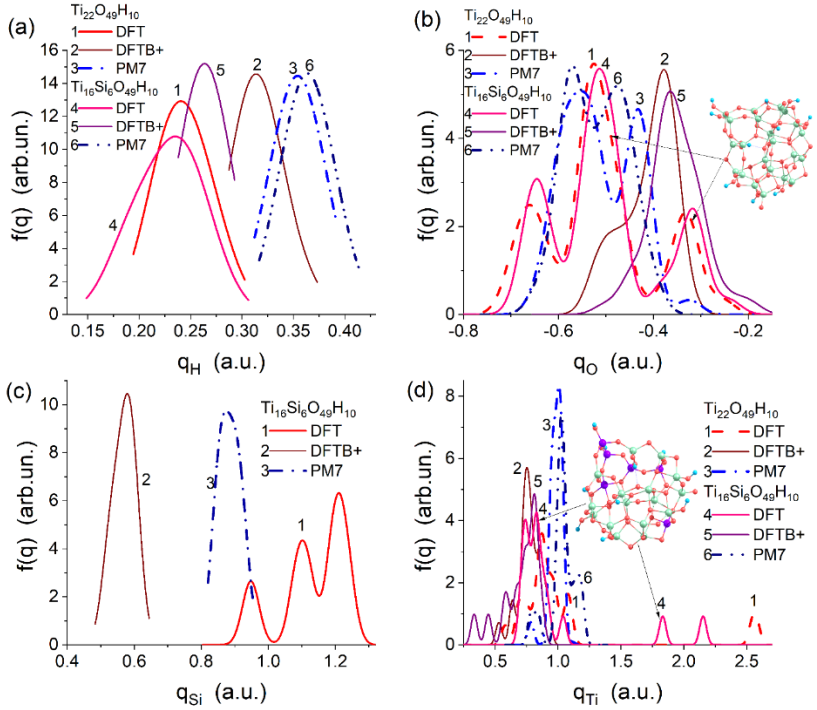

Fig. 4. Mulliken charge value distributions on (*a*) H, (*b*) O, (*c*) Si, and (*d*) Ti atoms in the clusters $Ti_{22}O_{49}H_{10}$ and $Ti_{16}Si_6O_{49}H_{10}$ calculated using DFT, DFTB+, and PM7 methods

Changes in the calculation methods result in much stronger changes in the CDF shapes (Figs. 3 and 4) than changes in the cluster compositions with solid solutions of alumina in silica (Fig. 5 *a*–*d*) or silica in titania (Fig. 5 *e*–*h*) (cluster models with 88 and 22 units, respectively). However, changes in CDF of Ti (Fig. 5 *h*) are much greater than that for Al because the difference between the atomic parameters of Si and Ti is greater than that between Si and Al. Therefore, for TS (solid solution of silica in titania with 4-6-O-coordinated Si atoms), the lattice stress could be much greater than that for AS. Therefore, the CDF for silica in AS (Fig. 5 *c*) are less dependent on the cluster composition than that for TS (Fig. 5 *g*). Additionally, the O CDF are more complex for TS (Fig. 5 *f*) than that for AS (Fig. 5 *b*). For the H CDF, the shape is more complex for AS (Fig. 5 *a*) than that for TS (Fig. 5 *e*) because of the adsorbed water and bridging hydroxyl contributions for AS.

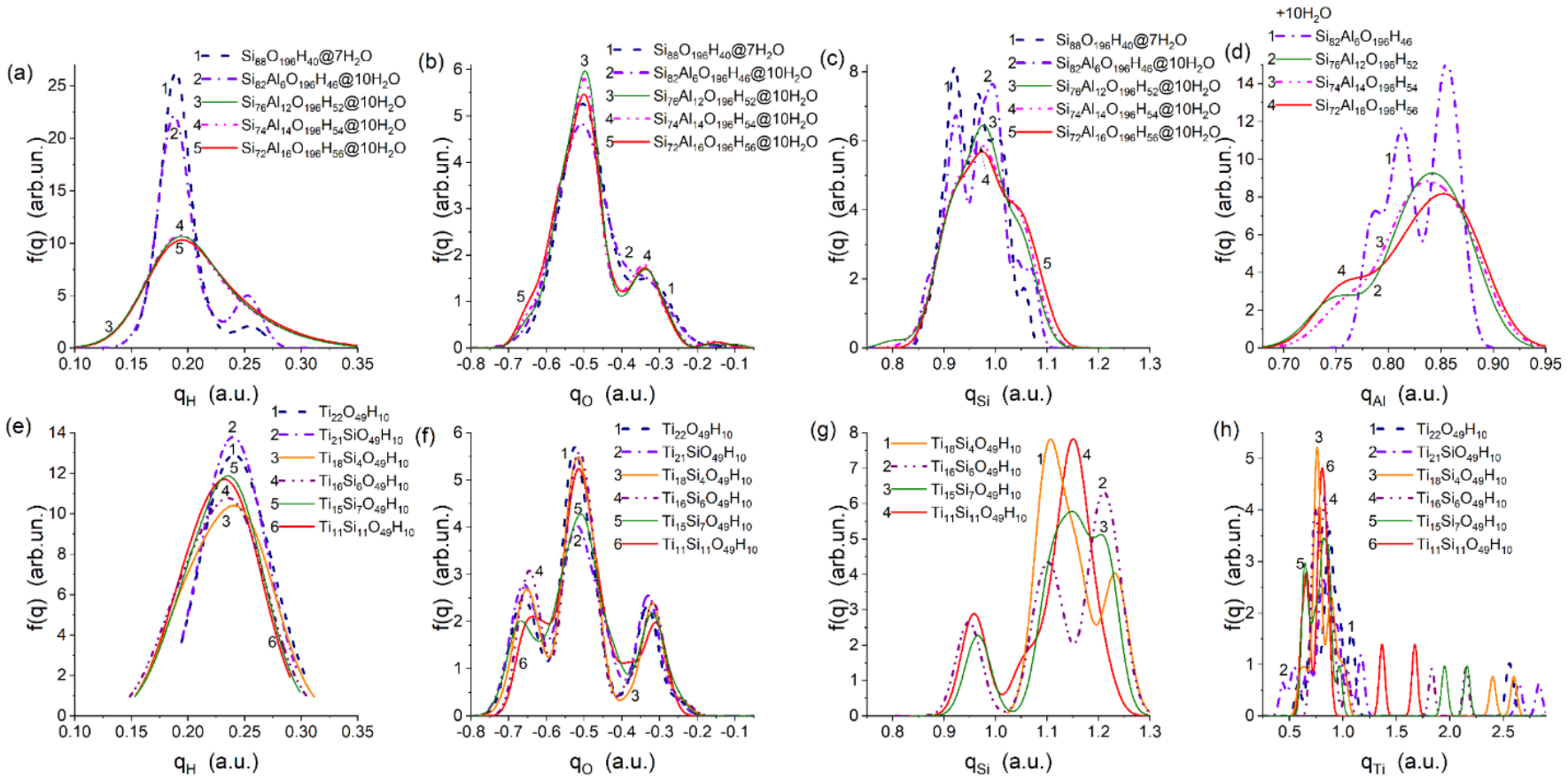

Fig. 5. Mulliken charge value distributions on (*a*, *e*) H, (*b*, *f*) O, (*c*, *g*) Si, (*d*) Al, and (*h*) Ti atoms in (*a*–*d*) AS and (*e*–*h*) TS clusters calculated using the ωB97X–D/cc–pVDZ method

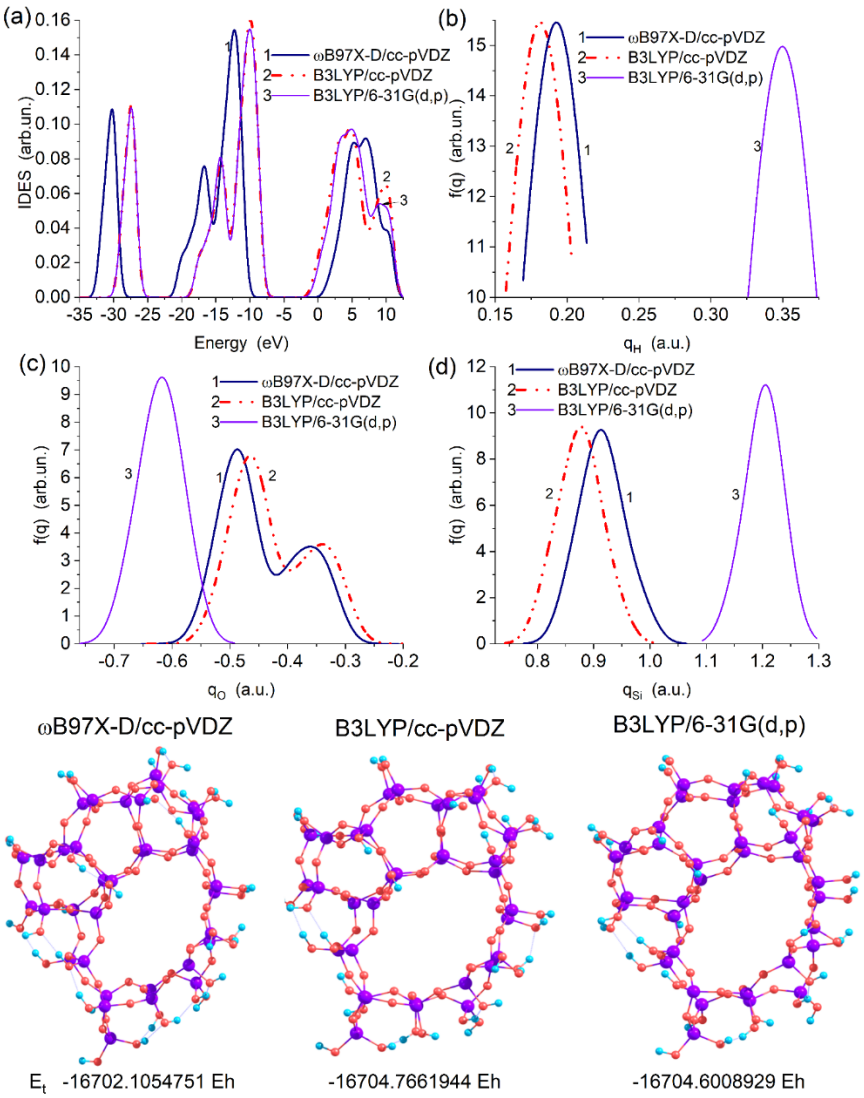

Fig. 6. DFT and basis set type effects on (*a*) IDES, and CDF of (*b*) H, (*c*) O, and (*d*) Si atoms in the silica cluster $Si_{35}O_{87}H_{34}$ calculated using ωB97X–D (curves 1) and B3LYP (2) with the cc–pVDZ basis set and B3LYP/6–31G(d,p) (3) (total energy E_t is shown in Hartree units)

The geometries of the silica cluster $Si_{35}O_{87}H_{34}$ calculated using ωB97X–D and B3LYP with the same basis set cc–pVDZ or B3LYP/6–31G(d,p) are similar (Fig. 6, bottom inserts). However, the atomic charges estimated using B3LYP are smaller (with cc–pVDZ) or larger (6–31G(d,p)) than that with ωB97X–D/cc–pVDZ (Fig. 6 *b*–*d*). For B3LYP, this causes the shift of VB toward higher energies and CB shifts toward lower energies but it is independent on the basis set type (Fig. 6 *a*). The E_g values from the B3LYP calculations are smaller (underestimated by *ca*. 1.4 and 1.6 eV) (Table 3) than that of ωB97X–D E_g value (overestimated by *ca*. 2.6 eV). Thus, the types of DFT and basis sets may strongly affect the VB/CB structure, and their appropriate selection could give better results for certain systems. Significant changes in the CDF of H, O, and Si atoms in the cluster $Si_{35}O_{87}H_{34}$ calculated using the B3LYP with cc–pVDZ and 6–31G(d,p) (Fig. 6 *b*–*d*) do not affect the IDES (Fig. 6 *a*). Thus, the CDF are more strongly depend on the basis set, but the IDES more strongly depend on the DFT type.

Water molecules bound to a surface of oxide clusters reduce the Gibbs free energy of the systems (Table 4), increase the bandgap, and stabilize the boundary levels (Tables 1–3). The latter effect is maximal for the γ–Al_2O_3 cluster with 111 units (Tables 1–3). For TS and AS and

especially for titania, the solvation effects (Table 4, ΔG_s) and water adsorption energy (ΔE_s for TS and AS) are much larger than that for amorphous silica. This explains why water is better adsorbed from air onto nanotitania, TS, and AS (characterized by abundance of uncompensated high surface energy reduced by the formation of surface hydroxyls upon dissociation adsorption of water and then by molecularly adsorbed water from air) than on pure nanosilica [6–8, 59].

Table 4. Adsorption energy of water and solvation effects for selected systems (ωB97X–D/cc–pVDZ with (ΔG_s) or without (ΔE_s) the SMD use)

Cluster	ΔE_s (kJ/mol)	ΔE_s per water molecule (kJ/mol)	ΔG_s (kJ/mol)
$Si_{88}O_{196}H_{40}$	–	–	–690.1
$Si_{88}O_{196}H_{40}@7H_2O$	–541.6	–77.3	–727.7
$Si_{82}Al_6O_{196}H_{46}@10H_2O$	–930.8	–93.1	–761.6
$Si_{82}Ti_6O_{196}H_{40}@7H_2O$	–1273.0	–181.9	–1207.9
$Ti_{22}O_{49}H_{10}$	–	–	−1688.7

CONCLUSION

It is well known that the bandgap, polarizability, conductivity, and dielectric characteristics play an important role in the application efficiency of oxide materials. Therefore, accurate determination of these characteristics is of interest from a practical point of view. Clear, the theoretical estimation of the characteristics is simpler, especially for large series of complex materials with varied compositions, by using QC methods (computations, no synthesis) than experimental ones (synthesis and measurements). Upon theoretical computations with QC methods, selection of a method adequate to a task is important to obtain correct information. Therefore, in this study, two semiempirical methods (PM7 and DFTB+ with very different parametrization methodology) have been used in parallel to DFT (mainly ωB97X–D with the cc–pVDZ basis set) to compute various clusters (22, 35, 88, 94, and 111 units) with silica, alumina, titania, titania/silica, and alumina/silica. The computations show that the E_g value of titania is accurately computed with DFTB+ using cluster and periodic boundary conditions approaches. However, for other systems, the DFTB+ method gives rather inaccurate, significantly underestimated E_g values (due to the pair parametrization problems for metal atoms used here). Typically, the PM7 and DFT methods give better values of $E_{g1} = E_{LUMO1} - E_{HOMO}$ (with smaller errors in comparison to the experimental values) using the potential approach V^{-1} (computation of the virtual levels of the systems with removed one electron) than the values of $E_g = E_{LUMO} - E_{HOMO}$ (overestimated). Detailed analyses of the integral density of electron states and density of atomic charges summarized by atom types reveal the reasons of nonmonotonic changes in the E_g values *vs*. composition of binary oxides computed by different methods. There are sometimes opposite changes in the atomic charges determining the location of the boundary energetic levels, and changes in the lattice stress and constants affecting the electronic structure of complex systems. However, the PM7 and DFT methods give correct tendencies in the E_g value changes *vs*. binary oxide compositions, but its values are overestimated in contrast to underestimated values by DFTB+. The DFT and basis set types can strongly affect the VB/CB structure, and their appropriate selection could give more accurate results for certain systems. Water adsorbed in a low amount on the oxide clusters provides significant stabilization of a surface since the Gibbs free surface energy strongly decreases. This explains effective adsorption of water from air even onto nonporous binary nanooxides or nanotitania in comparison to nanosilica.

It should be noted that the CDF method is original [58] and absent in any QC program suit. Additionally, in the literature, there is no detailed comparison of the computational results with DFT, PM7, and DFTB+ methods for silica, titatia, alumina, AS, and TS, which are important oxide materials from a practical point of view.

Thus, accurate selection of QC methods and material models allows one to obtain the results appropriate not only for qualitative but also for quantitative analyses of the experimental results and related phenomena. This is of importance for searching and creation of new and more effective materials for industry, medicine, *etc*. The use of appropriate theoretical methods and material models could simplify the mentioned processes.

ACKNOWLEDGMENT

The author is grateful to Gaussian, Inc. (USA) for the Gaussian 16, Revision C.02 and to the Vrije Universiteit (Amsterdam, The Netherlands) for AMS2023.1 and AMS2024.1 program suits.

Моделювання бінарних нанооксидів з твердих розчинів або змішаних фаз

В.М. Гунько

Інститут хімії поверхні ім. О.О. Чуйка Національної академії наук України
вул. Генерала Наумова, 17, Київ, 03164, Україна, vlad_gunko@ukr.net

Електронна структура індивідуальних оксидів металів (титану, алюмінію) або металоїдів (кремнію), а також складних (бінарних, потрійних) оксидів важлива з практичної точки зору, оскільки в різноманітних застосуваннях їх як каталізаторів, сорбентів, наповнювачів тощо, заборонена зона, поляризовність, діелектричні характеристики та провідність відіграють вирішальну роль у ефективності матеріалів. Тому вкрай необхідне точне визначення цих характеристик. Іноді визначення характеристик простіше, особливо для великих серій складних матеріалів із різноманітним складом, за допомогою теоретичних методів (обчислення, без синтезу), ніж експериментальних (синтез і вимірювання). Під час теоретичних обчислень (наприклад, з квантовохімічними методами) вибір методу, адекватного завданню, важливий для отримання правильної інформації. Тому в цьому дослідженні два напівемпіричні методи (PM7, DFTB+) використовувалися паралельно з DFT (ωB97X-D з базисом cc-pVDZ) для обчислення різних кластерів (22, 35, 88, 94 і 111 одиниць) з діоксиду кремнію, оксиду алюмінію, діоксиду титану, діоксиду титану/кремнезему і оксиду алюмінію/кремнезему. Обчислення показують, що ширина забороненої зони (E_g) діоксиду титану здебільшого точно обчислюється за допомогою DFTB+ з використанням кластерних або періодичних граничних умов. Однак для інших систем значення DFTB+ E_g є досить неточними (заниженими). Значення PM7 та DFT E_g є кращими з використанням потенціального підходу V^{-1} (обчислення віртуальних рівнів систем з видаленим одним електроном). Детальний аналіз інтегральної густини електронних станів і густини атомних зарядів, узагальнених за типами атомів, виявляє причини немонотонних змін значень E_g від складу бінарних оксидів. Загалом методи PM7 і DFT дають правильні тенденції у змінах значення E_g в залежності від складу бінарних оксидів, але його значення завищені, на відміну від занижених значень DFTB+. Вода, адсорбована в невеликій кількості на кластерах оксидів, забезпечує значну стабілізацію поверхні, оскільки вільна поверхнева енергія Гіббса сильно знижується, що пояснює ефективну адсорбцію води з повітря навіть на непористих бінарних оксидах або діоксиді титану в порівнянні з кремнеземом.

***Ключові слова**: бінарні нанооксиди, твердий розчин, змішані фази, електронна будова, метод ТФГ, напівемпіричні квантовохімічні методи*

REFERENCES

1. Somasundaran P. (editor). *Encyclopedia of Surface and Colloid Science*. Third Edition. (Boca Raton: CRC Press, 2015).
2. Advani S.G. *Processing and Properties of Nanocomposites*. (Singapore: Word Scientific Publising, 2007).
3. Birdi K.S. (editor). *Handbook of Surface and Colloid Chemistry*. Third edition. (Boca Raton: CRC Press, 2009).
4. Al-Abadleh H.A., Grassian V.H. Oxide surfaces as environmental interfaces. *Surf. Sci. Report*. 2003. **52**: 63.
5. Guo Z., Liu B., Zhang Q., Deng W., Wang Y., Yang Y. Recent advances in heterogeneous selective oxidation catalysis for sustainable chemistry. *Chem. Soc. Rev*. 2014. **43**: 3480.

6. Gun'ko V.M., Turov V.V. Nuclear Magnetic Resonance Studies of Interfacial Phenomena. (Boca Raton: CRC Press, 2013).
7. Gun'ko V.M., Turov V.V., Zarko V.I., Goncharuk O.V., Pakhlov E.M., Skubiszewska-Zięba J., Blitz J.P. Interfacial phenomena at a surface of individual and complex fumed nanooxides. *Adv. Colloid Interface Sci*. 2016. **235**: 108.
8. Gun'ko V.M., Turov V.V., Zarko V.I., Goncharuk O.V., Pakhlov E.M., Matkovsky O.K. Interfacial phenomena at a surface of individual and complex fumed nanooxides. *Surface*. 2019. **11(26)**: 3.
9. Schleyer P.v.R. (editor). *Encyclopedia of Computational Chemistry*. (New York: John Wiley & Sons, 1998).
10. Dykstra C.E., Frenking G., Kim K.S., Scuseria G.E. (editors). *Theory and Applications of Computational Chemistry, the First Forty Years*. (Amsterdam: Elsevier, 2005).
11. Cramer C.J. *Essentials of Computational Chemistry: Theories and Models*. Second edn. (Chichester, UK: John Wiley & Sons, Ltd, 2008).
12. Helgaker T., Jorgensen P., Olsen J. *Molecular Electronic Structure Theory*. *(New York:* John Wiley & Sons, 2014).
13. Martin R.M., Reining L., Ceperley D.M. *Interacting Electrons: Theory and Computational Approaches*. (Cambridge, UK: Cambridge University Press, 2016).
14. Engel E., Dreizler R.M. *Density Functional Theory: An Advanced Course*. (Berlin: Springer, 2013).
15. Yang K., Zheng J., Zhao Y., Truhlar D.G. Tests of the RPBE, revPBE, τ-HCTHhyb, ωB97X–D, and MOHLYP density functional approximations and 29 others against representative databases for diverse bond energies and barrier heights in catalysis. *J. Chem. Phys*. 2010. **132**(16): 164117.
16. Becke A.D. Perspective: Fifty years of density-functional theory in chemical physics. *J. Chem. Phys.* 2014. **140**(18): 18A301.
17. Stewart J.J.P. *MOPAC2022*. Stewart Computational Chemistry. web: HTTP://OpenMOPAC.net. 2024. (accessed on 30.01.2024, Ver. 22.1.1).
18. Hourahine B., Aradi B., Blum V., Bonafé F., Buccheri A., Camacho C., Cevallos C., Deshaye M.Y., Dumitrică T., Dominguez A., Ehlert S., Elstner M., van der Heide T., Hermann J., Irle S., Kranz J.J., Köhler C., Kowalczyk T., Kubař T., Lee I.S., Lutsker V., Maurer R.J., Min S.K., Mitchell I., Negre C., Niehaus T.A., Niklasson A.M.N., Page A.J., Pecchia A., Penazzi G., Persson M.P., Řezáč J., Sánchez C.G., Sternberg M., Stöhr M., Stuckenberg F., Tkatchenko A., Yu V.W.-z., Frauenheim T. DFTB+, a software package for efficient approximate density functional theory based atomistic simulations. *J. Chem. Phys*. 2020. **152**(12):124101.
19. Frisch M.J., Trucks G.W., Schlegel H.B., Scuseria G.E., Robb M.A., Cheeseman J.R., Scalmani G., Barone V., Petersson G.A., Nakatsuji H., Li X., Caricato M., Marenich A.V., Bloino J., Janesko B.G., Gomperts R., Mennucci B., Hratchian H.P., Ortiz J.V., Izmaylov A.F., Sonnenberg J.L., Williams-Young D., Ding F., Lipparini F., Egidi F., Goings J., Peng B., Petrone A., Henderson T., Ranasinghe D., Zakrzewski V.G., Gao J., Rega N., Zheng G., Liang W., Hada M., Ehara M., Toyota K., Fukuda R., Hasegawa J., Ishida M., Nakajima T., Honda Y., Kitao O., Nakai H., Vreven T., Throssell K., Montgomery J.A. Jr., Peralta J.E., Ogliaro F., Bearpark M.J., Heyd J.J., Brothers E.N., Kudin K.N., Staroverov V.N., Keith T.A., Kobayashi R., Normand J., Raghavachari K., Rendell A.P., Burant J.C., Iyengar S.S., Tomasi J., Cossi M., Millam J.M., Klene M., Adamo C., Cammi R., Ochterski J.W., Martin R.L., Morokuma K., Farkas O., Foresman J.B., Fox D.J. *Gaussian 16, Revision C.02*. (Gaussian, Inc., Wallingford CT, 2019).
20. Barca G.M.J., Bertoni C., Carrington L., Datta D., De Silva N., Deustua J.E., Fedorov D.G., Gour J.R., Gunina A.O., Guidez E., Harville T., Irle S., Ivanic J., Kowalski K., Leang S.S., Li H., Li W., Lutz J.J., Magoulas I., Mato J., Mironov V., Nakata H., Pham B.Q., Piecuch P., Poole D., Pruitt S.R., Rendell A.P., Roskop L.B., Ruedenberg K. Recent developments in the general atomic and molecular electronic structure system. *J. Chem. Phys.* 2020. **152**(15): 154102.
21. Rüger R., Franchini M., Trnka T., Yakovlev A., van Lenthe E., Philipsen P., van Vuren T., Klumpers B., Soini T. *AMS 2023.1*. SCM, Theoretical Chemistry, Vrije Universiteit, Amsterdam, The Netherlands, http://www.scm.com.
22. Cañas J., Alba G., Leinen D., Lloret F., Gutierrez M., Eon D., Pernot J., Gheeraert E., Araujo D. Diamond/γ-alumina band offset determination by XPS. *Appl. Surf. Sci.* 2021. **535**: 146301.
23. Alshoaibi A., Islam S. Mesoporous zinc oxide supported silica-titania nanocomposite: Structural, optical, and photocatalytic activity. *J. Alloys Compd.* 2021. **881**: 160582.
24. Paul P., Hafiz Md. G., Schmitt P., Patzig C., Otto F., Fritz T., Tünnermann A., Szeghalmi A. Optical bandgap control in Al_2O_3/TiO_2 heterostructures by plasma enhanced atomic layer deposition: Toward quantizing structures and tailored binary oxides. *Spectrochim. Acta, Part A.* 2021. **252**: 119508.
25. Somekawa S., Watanabe H., Ono Y., Oaki Y., Imai H. Preparation of titania with double band structure derived from a quantum size effect: Drastic increase in the photocatalytic activity. *Mater. Lett*. 2021. **304**: 130609.

26. Linsebigler A.L., Lu G., Yates J.T. Photocatalysis on TiO_2 surfaces: Principles, mechanisms, and selected results. *Chem. Rev.* 1995. **95**(3): 735.
27. Fujishima A., Hashimoto K., Watanabe T. *TiO_2 Photocatalysis Fundaments and Applications*. (Tokyo: University of Tokyo, BKC, Inc., 1999).
28. Emori M., Sugita M., Ozawa K., Sakama H. Electronic structure of epitaxial anatase TiO_2 films: Angle-resolved photoelectron spectroscopy study. *Phys. Rev. B.* 2012. **85**: 035129.
29. Umebayashi T., Yamaki T., Itoh H., Asai K. Analysis of electronic structures of 3d transition metal-doped TiO_2 based on band calculations. *J. Phys. Chem. Solid*. 2002. **63**(10): 1909.
30. Wang Y., Doren D.J. Electronic structures of V-doped anatase TiO_2. *Solid State Commun*. 2005. **136**(3): 142.
31. Wu H.-C., Li S.-H., Lin S.-W. Effect of Fe concentration on Fe-doped anatase TiO_2 from GGA + U calculations. *Int. J. Photoenergy*. 2012. **2012**(3): 823498.
32. Du Y., Wang Z., Chen H., Wang H.-Y., Liu G., Weng Y. Effect of trap states on photocatalytic properties of boron-doped anatase TiO_2 microspheres studied by time-resolved infrared spectroscopy. *Phys. Chem. Chem. Phys*. 2019. **21**(8): 4349.
33. Wischert R., Laurent P., Coperet C., Delbecq F., Sautet P. γ-Alumina: the essential and unexpected role of water for the structure, stability, and reactivity of "defect" sites. *J. Am. Chem. Soc*. 2012. **134**(35): 14430.
34. Landmann M., Rauls E., Schmidt W. The electronic structure and optical response of rutile, anatase, and brookite TiO_2. *J. Phys.: Condens. Matter*. 2012. **24**: 3.
35. Reyes-Coronado D., Rodriguez-Gattorno G., Espinosa-Pesqueira M.E., Cab C., Coss R.D., Oskam G. Phase-pure TiO_2 nanoparticles: anatase, brookite and rutile. *Nanotechnology*. 2008. **19**(14): 145605.
36. Rasalingam S., Kibombo H.S., Wu C.-M., Peng R., Baltrusaitis J., Koodali R.T. Competitive role of structural properties of titania–silica mixed oxides and a mechanistic study of the photocatalytic degradation of phenol. *Appl. Catal. B.* 2014. **148–149**: 394.
37. Kibombo H.S., Rasalingam S., Koodali R.T. Facile template free method for textural property modulation that enhances adsorption and photocatalytic activity of aperiodic titania supported silica materials. *Appl. Catal. B.* 2013. **142–143**: 119.
38. Worrall D.R., Williams S.L., Eremenko A., Smirnova N., Yakimenko O., Starukh G. Laser flash photolysis study of electron transfer processes of adsorbed anthracene on titania–silica surfaces. *Colloids Surf. A.* 2004. **230**(1–3): 45.
39. Ghaedi M. (editor). *Photocatalysis: Fundamental Processes and Applications*. Interface Science and Technology. V. 32. (Amsterdam: Elsevier, 2021).
40. Saleh T.A. (editor). *Surface Science of Adsorbents and Nanoadsorbents.* Interface Science and Technology. V. 34. (Amsterdam: Elsevier, 2022).
41. Suib S.L. *New and Future Developments in Catalysis. Catalysis by Nanoparticles*. (Elsevier, 2013).
42. Douhal A., Anpo M. *Chemistry of Silica and Zeolite-Based Materials. Synthesis, Characterization and Applications*. (Amsterdam: Elsevier, 2019).
43. Singh P., Bassin J.P., Rajkhowa S., Hussain C.M., Oraon R. (editors). *Environmental Sustainability and Industries. Technologies for Solid Waste, Wastewater, and Air Treatment.* (Amsterdam: Elsevier, 2022).
44. Fornasiero P., Cargnello M. (editors). *Morphological, Compositional, and Shape Control of Materials for Catalysis.* Studies in Surface Science and Catalysis. V. 177. (Amsterdam: Elsevier, 2017).
45. Abdulkadir B.A., Teh L.P., Abidin S.Z., Setiabudi H.D., Jusoh R. Advancements in silica-based nanostructured photocatalysts for efficient hydrogen generation from water splitting. *Chem. Eng. Res. Des*. 2023. **199**: 541.
46. Rashid R., Shafiq I., Gilani M.R.H.S, Maaz M., Akhter P., Hussain M., Jeong K.-E., Kwon E.E., Bae S., Park Y.-K. Advancements in TiO_2-based photocatalysis for environmental remediation: Strategies for enhancing visible-light-driven activity. *Chemosphere*. 2024. **349**: 140703.
47. Marenich A.V., Cramer C.J., Truhlar D.G. Universal solvation model based on solute electron density and on a continuum model of the solvent defined by the bulk dielectric constant and atomic surface tensions. *J. Phys. Chem. B.* 2009. **113**(18): 6378.
48. Cui M., Reuter K., Margraf J.T. Obtaining robust density functional tight binding parameters for solids across the periodic table. *ChemRxiv*. 2024. doi:10.26434/chemrxiv-2024-d0cff.
49. Pettersen E.F., Goddard T.D., Huang C.C., Meng E.C., Couch G.S., Croll T.I., Morris J.H., Ferrin T.E. UCSF ChimeraX: Structure visualization for researchers, educators, and developers. *Protein Sci.* 2021. **30**(1): 70.
50. *Avogadro 2*. https://two.avogadro.cc/. Ver. 1.99. 2024.
51. Pedretti A., Mazzolari A., Gervasoni S., Fumagalli L., Vistoli G. The VEGA suite of programs: a versatile platform for cheminformatics and drug design projects. *Bioinformatics*. 2021. **37**(8): 1174.
52. *Jmol: an open-source Java viewer for chemical structures in 3D* (Ver. 16.2.21), 2024. http://www.jmol.org/.
53. Gun'ko V.M. Modeling of interfacial behavior of water and organics. *J. Theor. Comput. Chem*. 2013. **12**(07): 1350059.

54. Gun'ko V.M. Interfacial phenomena: effects of confined space and structure of adsorbents on the behavior of polar and nonpolar adsorbates at low temperatures. *Current Physical Chemistry*. 2015. **5**(2): 137.
55. Gun'ko V.M. Effects of methods and basis sets on calculation results using various solvation models. *Him. Fiz. Tehnol. Poverhni.* 2018. **9**(1): 3.
56. Gun'ko V.M. Charge distribution functions for characterization of complex systems. *Him. Fiz. Tehnol. Poverhni.* 2021. **12**(1): 3.
57. Gun'ko V.M. Electronic structure of anatase doped by metals calculated using translational boundary conditions and cluster approach. *Him. Fiz. Tehnol. Poverhni.* 2014. **5**(2): 119. [in Russian].
58. Gun'ko V.M. Atomic charge distribution functions as a tool to analyze electronic structure of molecular and cluster systems. *Int. J. Quantum Chem*. 2021. **121**(14): e26665.
59. Gun'ko V.M., Zarko V.I., Goncharuk E.V., Andriyko L.S., Turov V.V., Nychiporuk Y.M., Leboda R., Skubiszewska-Zięba J., Gabchak A.L., Osovskii V.D., Ptushinskii Y.G., Yurchenko G.R., Mishchuk O.A., Gorbik P.P., Pissis P., Blitz J.P. TSDC spectroscopy of relaxational and interfacial phenomena. *Adv. Colloid Interface Sci.* 2007. **131**(1–2): 1.

Received 13.05.2024, accepted 05.03.2025